



Assessing the effects of CO₂/methane mixtures on gas–oil interfacial tension and fluid flow using compositional simulation

Paulo H. A. Dantas¹ · Ana L. N. dos Santos¹ · Igor E. S. Lins² · Gloria M. N. Costa² · Silvio A. B. Vieira de Melo^{2,3}

Received: 22 October 2022 / Revised: 28 March 2023 / Accepted: 31 March 2023 / Published online: 11 April 2023
© The Author(s) under exclusive licence to Associação Brasileira de Engenharia Química 2023

Abstract

In CO₂-enhanced oil recovery (CO₂EOR) processes, the gas–oil interfacial tension (IFT), which is a key property to determining oil recovery factor, affects rock wettability, capillary pressure, relative permeability, oil flow, and oil recovery factor (RF). The IFT is a key property when addressing the flow assurance issues in CO₂EOR processes, in which methane-rich gases mix with CO₂ for injection. Although the literature reports some studies on the effect of methane concentration on the properties of CO₂–oil systems, investigating methane content effects on IFT and fluid flow is still lacking, which is the primary motivation for the present work. Compositional simulations were carried out to evaluate the behavior of density, pressure, phase composition, oil saturation, IFT, and oil recovery to verify the effect in the IFT considering flow for different scenarios with varying methane concentration, pressure, and flow rate. The main focus is on the variation of these properties with IFT and their mechanisms. The results show how the methane content alters the CO₂ dissolution in oil, the light hydrocarbon extraction from the oil, the reservoir pressure, the phase densities, the oil saturation, the gas–oil IFT, and the RF. At the beginning of the process, an optimal methane concentration provides the maximum RF. However, the EOR process achieves the highest recovery in the long term by injecting only CO₂.

Keywords Enhanced oil recovery · CO₂ · Methane · Interfacial tension · Reservoir Simulation

Introduction

In recent years, enhanced oil recovery (EOR) methods have gained significant importance in the petroleum industry due to their capability to increase the oil recovery factor (RF). Generally, EOR organizes into primary, secondary, and tertiary – or enhanced – methods. Primary recovery takes

advantage of natural depletion due to the pressure difference between the reservoir and the production well. Secondary recovery, usually employed when the primary recovery is no longer effective, injects water, brine, or gas into the reservoir to maintain or increase the inner reservoir pressure. On the other hand, tertiary or enhanced recovery encompasses techniques such as chemical injection, ultrasonic stimulation, microbial injection, and thermal recovery aiming to produce additional effects other than pressure increase (Perera et al. 2016).

In the petroleum industry, processes such as gas–oil separation, multiphase flow, and oil extraction from reservoirs are influenced by IFT, which can be responsible for up to a third of the residual oil volume in petroleum reservoirs (Christensen et al. 2001). IFT also affects many other reservoir properties, such as wettability, permeability, and capillary pressure (Gajbhiye 2020).

Among the EOR techniques, CO₂ injection (CO₂EOR) is one of the most established and used worldwide (Islam 2019). This technique reduces oil viscosity and CO₂–oil interfacial tension and increases oil swelling, mobility, extraction, and sweep efficiency (Gu et al. 2013;

This is an invited, extended version of the manuscript presented at the 1st Flow Assurance Technology Congress and published in the FATC22 Proceedings.

✉ Silvio A. B. Vieira de Melo
sabvm@ufba.br

¹ Department of Chemical Engineering, Polytechnic School, Federal University of Bahia, Rua Aristides Novis, 2, Federação, Salvador, Bahia 40210-630, Brazil

² Graduate Program in Industrial Engineering, Polytechnic School, Federal University of Bahia, Rua Aristides Novis, 2, Federação, Salvador, Bahia 40210-630, Brazil

³ Interdisciplinary Center on Energy and Environment, Federal University of Bahia, Rua Barão de Jeremoabo, S/N, Campus de Ondina, Salvador, Bahia 40170-115, Brazil

Hemmati-Sarapardeh et al. 2014; Zanganeh et al. 2012). It also keeps the high internal reservoir pressure and an associated low cost (Shang et al. 2014). These factors generate a high displacement efficiency and decrease residual oil volume, thus improving the oil recovery. On the other hand, the increased CO₂ dissolution in oil leads to asphaltene precipitation (Zanganeh et al. 2012). From the flow assurance point of view, a trade-off between oil displacement and asphaltene precipitation due to CO₂ dissolution requires a technical and economic assessment of the process. The injection of other gases, such as methane or nitrogen, does not provide the same positive effects as CO₂ because these gases have a much lower solubility in oil (Ghaffar 2016).

Moreover, CO₂ injection benefits the environment since it mitigates greenhouse gas emissions. It is also helpful in the case of Brazilian pre-salt reservoirs, which naturally have a high-CO₂ content, reaching 40% (mol) in the produced gas (Carvalho et al. 2019). Although it is not within the scope of this work, the asphaltene and wax precipitation phenomena, as well as hydrate formation, dramatically affect the flow assurance in CO₂ injection processes and should be addressed appropriately.

The CO₂ injection into the reservoir can occur in miscible or immiscible conditions. Usually, immiscible CO₂ injection is less efficient and generates a low recovery factor (Hashemi Fath and Pouranfard 2014). The concept of miscibility refers to when the interfacial tension between two phases approaches zero and no more interface occurs between the phases (Gu et al. 2013). For gas–oil systems, there is usually a minimum pressure at a given temperature at which the reservoir oil and the injection gas become miscible. It is called the minimum miscibility pressure (MMP) (Choubineh et al. 2019).

Miscibility can be achieved at pressures above the MMP through condensation, vaporization, or a combination of both mechanisms (Zick 1986). The first-contact miscibility occurs when the oil and the injected gas reach miscibility upon their first contact in the reservoir at any arbitrary rate. However, in most cases, gas–oil miscibility develops through continuous mass transfer between the phases, named multi-contact miscibility (Choubineh et al. 2019; Green and Willhite 2018).

In the case of CO₂–oil systems, the multi-contact miscibility depends on mass transfer and phase equilibrium between the liquid and gas phases (Zhang et al. 2018). When considering the oil flow resulting from CO₂ injection, as soon as the oil and gas come into contact, the processes of CO₂ dissolution in oil (condensation mechanism) and the extraction of the light components from the oil by CO₂ (vaporization mechanism) occur. After the first contact, the injected CO₂ – now enriched with hydrocarbons extracted from the oil – advances along the reservoir due to its higher mobility and encounters the fresh oil, i.e., the

oil that has not met the CO₂ front yet, further increasing its enrichment. Thus, after multiple contacts, the enriched CO₂ becomes miscible in the oil (Gu et al. 2013). This process promotes a change in the compositions and properties of the CO₂–oil system, such as density, viscosity, and interfacial tension (IFT) (Cho et al. 2020).

However, in practice, the injected CO₂ is often mixed with various components due to the different sources of the injected gas, such as light hydrocarbons, sulfur, and nitrogen compounds, which affect the performance of the injection process. As the purification of the CO₂ streams is quite expensive, the injection of CO₂ mixed with some other components leads to a significant cost reduction in the CO₂ EOR processes (Shokrollahi et al. 2013). Among these components, methane gas is generated as a product of primary, secondary, and tertiary oil extraction processes and used as a reinjection gas for EOR processes. Therefore, it is the object of study of the present work. It is imperative to understand these components' effects on the injection performance of an EOR method to determine whether it is appropriate to inject a CO₂ stream into the reservoir without purification (Jin et al. 2017) since gas purification has a high cost, which, if avoided, contributes to the economic performance of the injection.

Several authors have studied the effect of CO₂ + methane injection on the IFT and MMP of CO₂–oil systems. Choubineh et al. (2019), Gu et al. (2013) and Zhang et al. (2004) observed that the MMP increases as methane concentration in the injected gas increases. According to them, this occurs because methane has a solubility in oil and an ability to extract light components much lower than CO₂, which makes it difficult for the system's phases to reach miscibility. Zhang et al. (2018) compared the properties of CO₂–oil systems with and without methane and reported that the increase in the system's pressure generates a slight increase in oil density due to CO₂ dissolution in oil. However, as methane is a much lighter gas than CO₂, the CO₂ + methane dissolution in oil causes the opposite effect: decreased oil density with increased pressure.

The literature reports several studies on oil recovery using CO₂, with and without methane (Ghaffar 2016), and the impact of the methane concentration in CO₂ on the properties of the CO₂–oil system. However, most of these studies end up focusing just water alternating CO₂ injection (CO₂WAG), instead of injecting only CO₂, as is the case of Cho et al. (2020) and Ghaffar (2016), so it is not possible to make a direct comparison between them and the present work. The higher the methane content in the CO₂ injection stream, the smaller the amount of oil recovered at the end of the process (Cho et al. 2020; Ghaffar 2016) noted that a 0 to 50% increase in methane molar fraction reduced the RF by about 36% at 21 °C and 650 psi.

Jin et al. (2017) studied the effect of methane concentration in the CO₂ injection stream on a water alternating gas (WAG) process. Jin et al. (2017) also reported that, for the case under study, after the injection of four pore volumes of CO₂ in the reservoir, the oil RF reached its maximum value when the methane content in the injection gas was between 10 and 20%. However, regardless of the injected pore volume, when the methane content in the injection gas reached 40%, the flow changed from miscible to immiscible. It indicates that the injection gas has an optimum composition range in the initial periods of the process, which leads to maximum recovery while reducing costs since CO₂ purification is unnecessary. However, the optimum composition range for a continuous gas injection in a WAG process is not reported in the literature. Moreover, studies on continuous gas injection processes performed under the same conditions used by Jin et al. (2017) have not been found in the literature.

Cho et al. (2020) studied the effects of methane concentration by simulating a WAG injection process in an oil reservoir. They observed that a higher methane concentration leads to less gas dissolving in the oil, reducing its viscosity. Consequently, the fraction of the injected gas does not create preferential gas channels, which could lead to an early breakthrough of the produced gas. Zhao and Yu (2018) reported a strong correlation between the methane content on a CO₂ stream and the breakthrough pressure, in a way that the higher the content, the higher the IFT and the breakthrough pressure. In addition, due to its low solubility in water, methane suffers a breakthrough before CO₂. Cho et al. (2020) also noted that, during the first cycle of WAG injection, the reservoir's average gas saturation increases with the methane concentration since it occupies a greater pore volume than CO₂. However, due to the low sweeping efficiency promoted by methane, this trend reverses in the following cycles, similar to those observed by Ghaffar (2016). Thus, the sum of the effects of sweeping efficiency, displacement efficiency, and compressibility increases the oil recovery factor with the methane concentration in the early stages of the WAG process. However, in the following WAG cycles, the observed trend is reversed, and oil recovery becomes greater for CO₂ injection.

Nobakht et al. (2007) performed an experimental analysis of the impact of IFT and other variables on a CO₂EOR process. The authors observed that, at pressures lower than a certain threshold, the IFT reduces linearly with the increasing pressure, whereas, above this threshold, the IFT continues to reduce but with a much smaller trend. Such behavior was attributed to the fact that, at low pressures, the pressure increase leads to a rise in CO₂ dissolution in oil, which quickly reduces the IFT. However, at high pressures, the light components extraction process begins, which leads to a change in the oil phase composition, and explains the difference in the IFT curve behavior. The authors also compared

the direct impacts of the injection pressure on the CO₂EOR and found similar trends. At low values of injection pressure, the CO₂EOR is low and almost constant because of the low CO₂ viscosity, the high IFT, and the high capillary force, which leads the injected CO₂ only to displace the oil from the largest pores. At medium values, the CO₂ viscosity increases and quickly dissolves into the oil, lowering the IFT and equilibrating the capillary and viscous forces, leading to higher CO₂EOR. Finally, at high values, the residual oil remains only in the smallest pores where the viscous force is not strong enough to displace. Consequently, the CO₂EOR reaches a maximum and becomes almost constant again.

Drexler et al. (2020) studied the effects of CO₂ dissolution on both dynamic and equilibrium IFT between a high-salinity brine and a Pre-salt oil with a high total base number (TBN), a non-negligible total acid number (TAN), and a considerable amount of asphaltene and resins. Although the CO₂ dissolution decreased the time required for the IFT to reach equilibrium by 70%, the authors observed it did not reduce the IFT. Thus, oil recovery depends on viscosity reduction and wettability alteration. Analyzing the impact of the pH on the IFT, the authors also found that for neutral and basic pH values, the IFT values remained constant, while, for strongly acid pH, the IFT reached the maximum values.

Recently, Abdullah and Hasan (2021) studied the effects of miscible CO₂ injection on a CO₂EOR process. However, the authors did not carry out an approach as complete as the one presented in this work. For pure CO₂ injection, increasing the reservoir pressure and the temperature raises oil production through IFT reduction, oil swelling, reducing oil viscosity, increasing sweep efficiency, increasing CO₂–oil interaction, and other mechanisms related to supercritical CO₂.

There are several methods to measure the IFT experimentally, so the most established one is the pendant drop method. This method determines the IFT by photographing a pending droplet and measuring the drop dimensions from the negative films. Currently, the most employed method for measuring IFT is the axisymmetric drop shape analysis (ADSA) technique, an improvement of the pendant drop method improved by Cheng et al. (1990).

Many authors developed different methods to calculate the IFT as a function of specific variables. Therefore, several empirical, semi-empirical, and phenomenological methods can determine the IFT in multicomponent systems. Among the CO₂–oil systems, the most used in general, including numerical simulation purposes, is the Parachor method, developed by Weinaug and Katz (1943), due to its simple formulation, even though this method frequently leads to higher deviations compared to others. Other more complex methods, but less used, are the density gradient theory (DGT) (Cahn and Hilliard 1958), the linear gradient theory (LGT) (Zuo and Stenby 1996), and the theory of the

corresponding state (Zuo and Stenby 1997). Such methods are not commonly used because they require complex mathematical treatments, which are unfeasible for reservoir numerical simulation since they require high computational efforts (Pereira 2016).

In the literature, to our knowledge, no work compares the injection of CO₂ with and without methane, analyzing the impact of the methane content on the system's properties, especially on the gas–oil IFT and the oil recovery factor. Cho et al. (2020) performed a similar analysis but for the cycles of a WAG process, not a gas-only injection one. Jin et al. (2017) also analyzed a WAG process but did not evaluate the effects of the systems' properties. Ghaffar (2016) did not assess its impact on the IFT, although they compared CO₂ injections with and without methane.

The experimental measurements of IFT and studies about the effect of this property on the gas–oil system generally consider only motionless systems, i.e., an oil droplet surrounded by gas, typical of the experimental setup. The present work, however, performs an assessment that is more representative of the CO₂ EOR processes, considering the effect of the IFT throughout the oil flow inside the reservoir, which is a novelty in the literature.

Until now, the analyzed IFT values were obtained by experimental procedures, such as the pendant drop method. In this case, the characteristics of the reservoir in the IFT and oil displacement and recovery are not assessed. For such, simulations were carried out considering different methane concentrations in the injection gas, ranging from 0 to 50% molar of methane in a mixture with CO₂. In addition, other injection conditions are tested, such as gas injection at constant pressure, considering pressure values above and below the experimental MMP, and gas injection at a constant flow rate. For each simulation, the behavior of various properties of the gas–oil system along with the flow is compared, such as density, pressure, phase composition, oil saturation, and, of course, IFT and oil recovery. The focus is on the variation of these properties that affect the IFT and the mechanisms involved.

This kind of analysis is not found in the literature at all. Still, it is reasonably necessary due to the role of IFT on fluid displacement in a porous medium and its intimate relationship with the properties of the CO₂–oil system, besides the flow assurance issues.

Methodology

The present work simulated CO₂ injection for different CO₂ and methane mixtures through the numerical simulator Generalized Equation-of-State Model Compositional Reservoir Simulator (GEMTM), developed by the Computer Modelling Group (CMG).

A field-scale optimization study in a more realistic scenario as performed, for example, using open-source carbonate benchmarks that represent Brazilian pre-salt field trends, as presented in UNISIM-IV, is not our goal. The main focus is to investigate the effect of the gas–oil interfacial tension considering the compositional flow for different scenarios with varying methane concentration, pressure, and flow rate.

The GEMTM is a reservoir simulator for compositional, chemical end unconventional modeling, describing the multidimensional and multiphase flow through porous media considering phase behavior and mass transfer. It accurately models the flow of three-phase, multicomponent fluids and primary, secondary, and tertiary recovery processes, mainly enhanced oil recovery processes. For this, the balanced system equations consider Darcy's law and mechanical dispersion and diffusion. CO₂ solubility in the water phase, which is an important aspect of CO₂EOR, is regarded by Henry's law. The oil data were taken from Sequeira et al. (2008), and the reservoir model proposed by Killough and Kossack (1987) was adopted. These are the unique papers in the literature that reported both PVT and CO₂–oil IFT data, which is the property of most significant interest in the present work.

Oil characterization

Before running the simulations, it is required to characterize the oil and define the reservoir's characteristics properly. The PVT characterization of the oil was carried out using experimental data of saturation pressure, separator test, constant composition expansion, differential liberation, swelling test, and MMP, all provided by Sequeira et al. (2008) for CO₂–oil systems. Table 1 shows the oil composition used in the simulations, molar weight and density. More information about the PVT characterization of the oil can be found in Section A in Supplementary Information, such as which PVT experiments were analyzed and details about the equations used for modeling.

Table 2 presents the minimum, maximum and average deviations obtained in describing the oil's PVT properties using WinProp[®] 2019.1. The modeling used to describe the experimental data obtained from Sequeira et al. (2008) showed acceptable numerical deviations for performing the numerical simulation of the CO₂ injection, with the average deviation being less than 1% for most of the described properties.

Reservoir modeling

Table 3 presents the characteristics of the numerical grid used in the simulations, while Table 4 shows the reservoir properties. The grid used to describe the reservoir

Table 1 Composition and properties of the original oil

Component	Molar Content (%)	Component	Molar Content (%)
CO ₂	0.0361	iC ₅	0.822
N ₂	0.0226	nC ₅	0.786
C ₁	23.735	C ₆	2.644
C ₂	0.00877	C ₇₊	71.423
C ₃	0.0638	Molar weight (g/mol)	164.50
iC ₄	0.117	Density, at 1250 psi and 15.56 °C (kg/m ³)	740.3
nC ₄	0.342		

Adapted from: Sequeira et al. (2008)

Table 2 PVT properties described in the oil PVT modeling stage and the respective deviations obtained

Property	Minimum deviation (%)	Maximum deviation (%)	Average deviation (%)
Saturation pressure (23.89 °C)	–	–	0.35
Saturation pressure (114.44 °C)	–	–	0.60
Relative oil volume	0.00077	0.40	0.091
Oil density	0.019	0.50	0.14
Oil compressibility	0.0023	0.38	0.16
Gas–oil ratio	0.067	22.62	2.26
Gas compressibility factor	0.085	1.25	0.65
Gas formation volume factor	0.060	2.12	0.81
Gas specific gravity	0.29	14.71	2.94
°API of the oil	0.13	0.17	0.15
Oil viscosity	0.050	2.39	0.91
Saturation Pressure	0.024	1.65	0.86
Swelling factor	0.11×10^{-14}	0.86	0.48
MMP	–	–	3.93

Table 3 Reservoir properties by layer

Layer	Horizontal permeability (mD)	Vertical permeability (mD)	Thickness (m)
1	500	50	6.096
2	50	50	9.144
3	200	25	15.240

Adapted from: Killough and Kossack (1987)

has $7 \times 7 \times 3$ dimensions. The injector and producer wells were positioned in blocks (1, 1, 3) and (7, 7, 1), respectively, so there is the greatest possible distance between them.

As seen in Table 4, both the present work and Killough and Kossack (1987) consider the presence of formation water in the reservoir, seeking to approximate the modeling to a more realistic case. However, the objective of the present work does not concern the study of the effect of this water. Thus, it is assumed to be pure water without

Table 4 General reservoir properties

Properties	Values
Reservoir length and width	152.4 m
Grid dimensions	$7 \times 7 \times 3$
Rock compressibility	$5.0 \cdot 10^{-6}$ psi ⁻¹
Reference depth	285 m
Initial pressure at the reference depth	6680 psi
Temperature	114.44 °C
Initial oil saturation	0.8
Initial water saturation	0.2
Porosity	0.3

Adapted from: Killough and Kossack (1987)

dissolved salts to simplify the simulations. Neither the dissolution of gases in water nor geochemical reactions between oil, water, and rock are considered.

Gas–oil IFT modeling

The GEM™ compositional simulator calculates the CO₂–oil IFT using the Parachor method for multicomponent systems. The Parachor parameter of the system's pseudo components is calculated by Firoozabadi et al. (1988).

Simulations

Simulations using the compositional simulator GEM ensure an accurate description of the flow assurance issues. GEM can consider essential phenomena such as asphaltene precipitation and better describe the phase and interfacial behavior effects than black oil simulators. Various injection process restrictions were established for each simulation, as shown in Table 5. Besides, for each set, the following CO₂ compositions were chosen: low-methane content CO₂ stream (100% CO₂), medium-methane content CO₂ stream (75% CO₂ and 25% methane), and high-methane content CO₂ stream (50% CO₂ and 50% methane), all in molar fraction.

For the first set of simulations, the bottom hole pressure (BHP) restriction was defined in the injector and producer wells. The injector BHP was set at 7000 psi, a pressure higher than the pure CO₂–oil system MMP reported by Sequeira et al. (2008) and described during the oil PVT characterization, which was 6675 psi. This was done to guarantee that the reservoir's internal pressure does not reach a value lower than the experimental MMP. However, the pressure drop across the reservoir may cause the pressure in the producing well to drop below this value. The producer BHP was set at 6500 psi to avoid a huge pressure difference between the wells and thus keep the oil recovery values within a feasible range. As the injection gas composition directly affects the MMP of a gas–oil system, the new MMP value should be calculated for CO₂ + methane injection cases, and then the BHP values based on this adjustment should be selected. However, the correlations available in the literature to compute the MMP of the CO₂–methane–oil systems were developed considering low methane concentrations. There is no consensus between the MMP values calculated by simulation and correlations. So, for each simulation set, the

same restrictions in the BHP and the wells' surface gas rate (STG) values were chosen, regardless of the composition of the injection gas. For the second set of simulations, the injector BHP was defined as 6000 psi, below the calculated MMP for pure CO₂, aiming to assess the effect of immiscible flow on the process. The producer BHP was set at 5500 psi for the same reason. For the third set of simulations, STG of the injector and producer BHP values were chosen as restrictions. The STG was set at 12,000 MCF/day, the same value used by Killough and Kossack (1987), while the BHP remained the same as in the first set. The purpose is to compare the process results when the injection is performed under both fixed pressure and fixed flow conditions and to assess the influence of these approaches on the IFT calculation and, consequently, on the oil recovery factor.

Results and discussion

First, it is analyzed the behavior of the properties of the mixtures CO₂–methane–oil system as a consequence of the mechanisms of gas dissolution in oil and light components extraction. Then, the effect of these properties on the system's IFT and, subsequently, their impacts on the field oil recovery are evaluated. As the properties of a CO₂–oil system depend on position and time, to analyze them over time, a block of the reservoir grid was first defined to be observed. Since the grid was discretized as 7 × 7 × 3, it was decided to examine the properties of the intermediate block in position (4, 4, 2), located precisely in the reservoir center. To facilitate the understanding of the simulations, Fig. 1 illustrates the reservoir grid, highlighting the position of the injector and producer wells and the intermediate block under analysis.

Analysis of the behavior of the system's properties

Figure 2 compares the molar fraction of CO₂ in oil over time for the three sets of simulations and each injected gas composition. The higher the methane content in the injected CO₂, the lower the molar fraction of dissolved CO₂. Similar

Table 5 Simulation conditions

	First set – above MMP	Second set – bellow MMP	Third set – con- stant injection flow rate
Injector well surface gas rate (14.7 psi, 60 °F) (STG)	–	–	12,000 MCF/day
Injector well bottom hole pressure (BHP)	7000 psi	6000 psi	–
Producer well bottom hole pressure (BHP)	6500 psi	5500 psi	6500 psi
Maximum simulation time	30 years	30 years	30 years

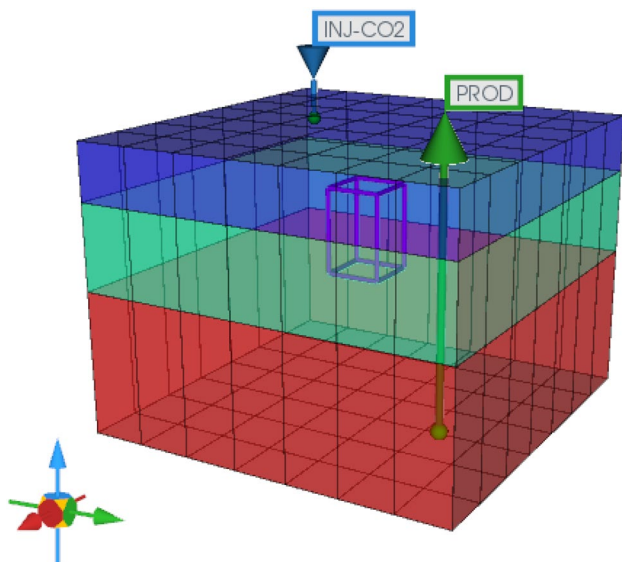


Fig. 1 Illustration of the grid used for the reservoir modeling, highlighting the positions of the injector and producer wells and also the intermediate block under analysis

results were reported by Ghaffar (2016). This effect also impacts the MMP of the system, as observed by Choubineh et al. (2019), who stated that the higher the methane content in the injected CO_2 , the greater the MMP of the mixture CO_2 –methane–oil system.

Looking at Fig. 2, it is also possible to notice that the curves for all cases show similar behaviors. At the beginning of the injection process, the CO_2 molar fraction in oil is zero, as the injected gas has not yet had time to reach the intermediate block under analysis. However, around 1989,

the curves went up and stabilized at the first level until they presented a new abrupt growth and finally stabilized at a final level. When the injected CO_2 meets the oil, a displacement front, composed of oil and dissolved CO_2 , is formed, which leads to a diffusion process that allows CO_2 to propagate from the front to the fresh oil, even if there is no direct contact between the fresh oil and the gas phase. The first growth of the CO_2 molar fraction curves represents this diffusion process. The first level represents the state in which the diffusion of CO_2 in the oil reached its maximum value.

On the other hand, the second growth of the curves means the moment when the gas phase reaches the oil. Comparing the CO_2 + methane injections simulated at a fixed pressure, as seen in Fig. 2a and b, the curves reach a stability level earlier for the case of gas injection at a pressure above the MMP, i.e., the systems with gas injection at higher pressures come to the equilibrium state more quickly. Figure 2c shows that, in addition to the curves corresponding to a stability level more rapidly than the other cases, after stabilizing, the curve for pure CO_2 injection exhibited an abrupt growth in 2013 until reaching a new level. This anomalous behavior is dealt with in further detail in this work since the analysis of the oil phase composition alone cannot explain this behavior.

Table 6 presents the CO_2 molar fraction in oil at the end of the simulation time for each injection gas composition and each simulation set. In addition, Table 6 facilitates the comparison of results for each simulation set. It allows observing that the highest CO_2 molar fractions in oil always occur for the third set of experiments, followed by the first and the second.

Figure 3 was built to analyze the light hydrocarbon extraction from the oil by the CO_2 -rich gas phase for the

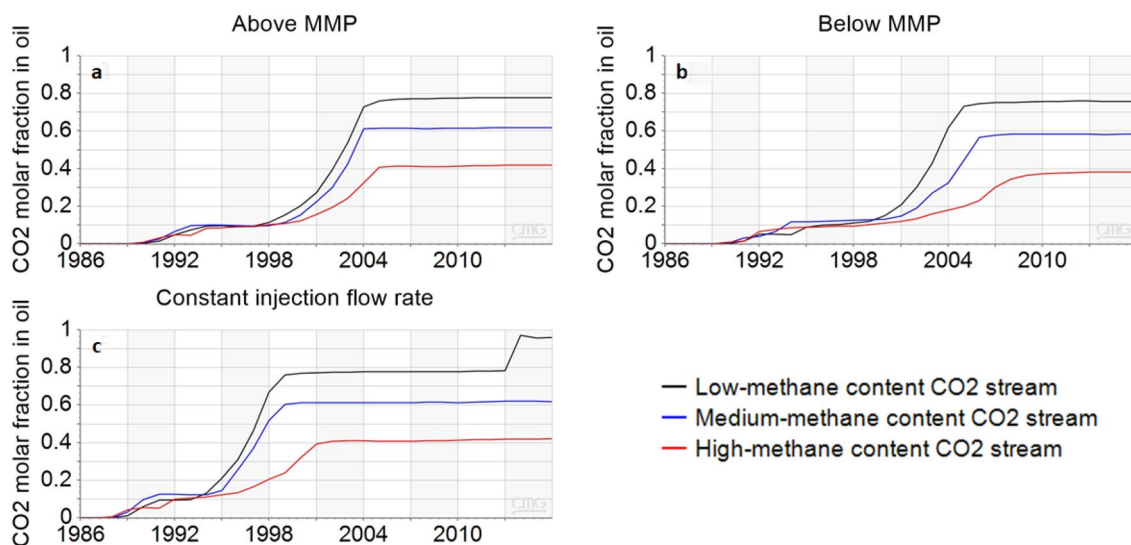
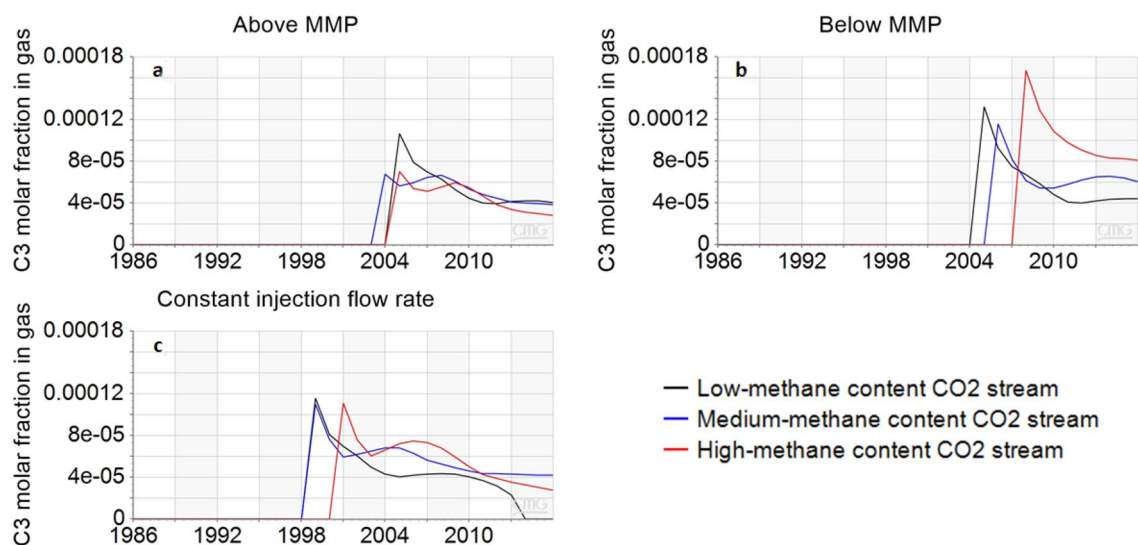


Fig. 2 CO_2 molar fraction in the oil over time in the block (4, 4, 2), considering the three sets of simulations and the three different methane concentrations in the CO_2 injection stream

Table 6 CO₂ molar fraction in oil at the end of the simulation time

Injection gas composition	First set –Above MMP (%)	Second set – Bellow MMP (%)	Third set – Constant injection flow rate (%)
100% CO ₂	77.70	75.92	95.90
75% CO ₂ + 25% CH ₄	61.92	58.40	61.95
50% CO ₂ + 50% CH ₄	41.95	38.22	42.07

**Fig. 3** Gas mole fraction of extracted C₃ over time in the block (4, 4, 2), considering the three sets of simulations and the three different methane concentrations in the CO₂ injection stream

three different injection gas streams: two with methane in their composition and one with pure CO₂. To do so, it was necessary to analyze one of the light components of the oil. Although methane (C₁) would be the adequate choice, it is impossible to directly monitor how much of it is being extracted from the gas phase because this component is being injected into the system along with the CO₂. The second option is to monitor the concentration of C₂. However, as shown in Table 1, the molar fraction of this component in the oil is very close to zero. Therefore, the C₃ component was chosen to analyze hydrocarbon extraction from the oil to the gas phase.

In Fig. 3, a direct relationship between the methane concentration and the extracted fraction is not observed, which contraries the results of Zhang et al. (2018), who reported that the increase in the methane content led to a decrease in extraction. The most likely cause of this divergence is the differing methodologies adopted. While Zhang et al. (2018) considered all hydrocarbons extracted from oil, the present work considered the extraction of only C₃. A comparison of Figs. 2 and 3 shows that the extracted C₃ molar fraction curves reach a value other than zero and their maximum values at the same time as the respective CO₂ dissolved in

oil molar fraction curves reach their final constant levels. This behavior again corroborates the work of Zhang et al. (2018). Therefore, the results of Figs. 2 and 3, together with those of Zhang et al. (2018), indicate that the light component extraction mechanism only significantly influences the system when the CO₂ dissolution mechanism no longer matters. Although the diffusion process guarantees that the CO₂ molecules propagate to the fresh oil in the block under study, the amount of CO₂ that dissolves in the fresh oil due to this process is very small, as shown in Fig. 2, which does not provide the formation of a gas phase. The gas phase only appears in the system when the injected gas reaches the block under study and consequently, while the meeting between these phases does not occur, the curves in Fig. 3 present a null value. Therefore, the point at which the molar fraction of C₃ ceases to have a zero value corresponds to the moment when the injected gas reaches the block. Analyzing Fig. 3c in detail, one notes that the curve for pure CO₂ injection presents an abrupt drop to zero, again, in 2013, a behavior discussed in detail later. Information about the pressure for the block (4, 4, 2) and the gas rate SC over time can be found in Fig. S2 and Fig. S3, respectively, in Section B in Supplementary Information. To facilitate the understanding

of the methane concentration effects on the internal pressure of the reservoir, Fig. 4 magnifies Fig. S2 to improve the visualization for only the cases of injection above and below the MMP. Figure 4 shows that the higher the methane content in the injection gas, the higher the pressure in the block (4, 4, 2). These findings are in line with the results obtained by Cho et al. (2020), although these authors have studied cases of the water alternating gas (WAG) process. This occurs because methane has lower compressibility than CO₂, thus contributing to keeping the reservoir pressure stable (Cho et al. 2020), in contrast to CO₂, which promotes a pressure drop when dissolved in oil. Information about the phases' densities and the oil saturation over time can be found in Fig. S4 and Fig. S5, respectively, in Section C in Supplementary Information.

Analysis of the system's IFT

Figure 5 presents the gas–oil IFT curve over time for the three sets of simulations and the three different methane concentrations in the CO₂ injection stream. Although the IFT values shown in Fig. 5 seem relatively low, Sequeira et al. (2008) observed that for the same oil in a condition of pure CO₂ injection at 6000 psi, the IFT presented values as low as 0.01 mN/m. As the injection conditions are close to those considered in the present work, it is concluded that the IFT values found are consistent. It is also possible to notice that, after leaving the null value, the IFT curves quickly stabilize, showing that, after the gas reaches the block, the IFT does not vary significantly

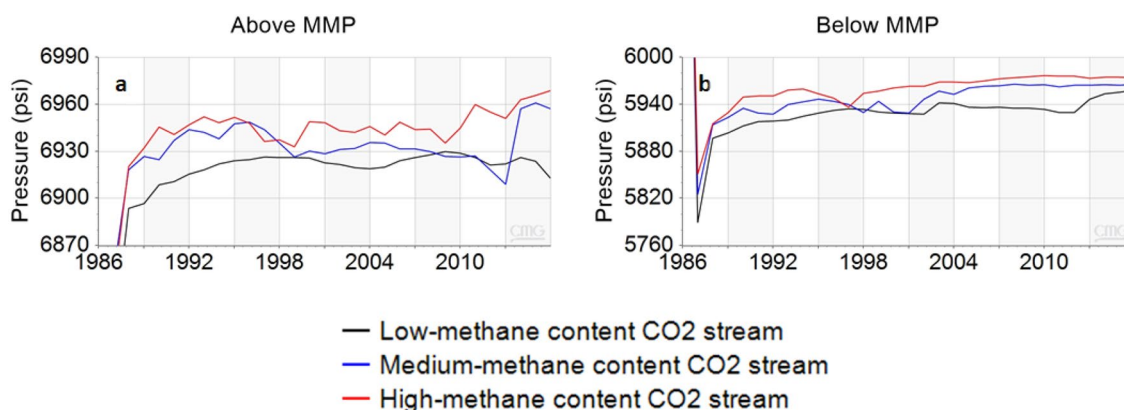


Fig. 4 Pressure over time in the block (4, 4, 2), considering only the first and second sets of simulations and the three different methane concentrations in the CO₂ injection stream

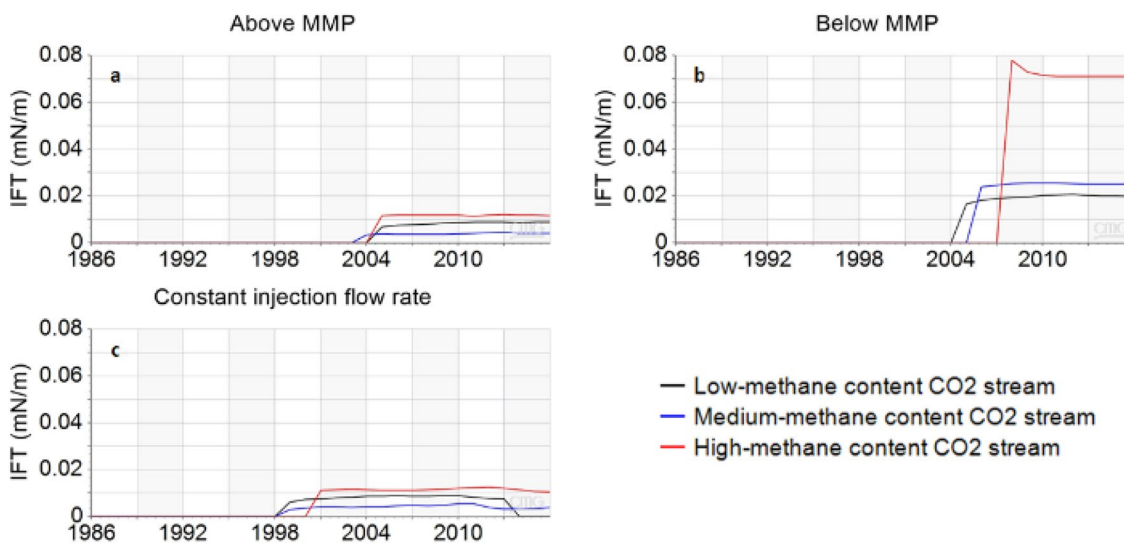


Fig. 5 Gas–oil interfacial tension overtime in the block (4, 4, 2), considering the three sets of simulations and the three different methane concentrations in the CO₂ injection stream

over time, except for pure CO₂ injection in Fig. 5c. This behavior is discussed in detail later. This point indicates that the oil reaches saturation with the injected CO₂, which can be observed by analyzing both Figs. 2 and 5 and noting that the curves reach stability simultaneously.

When observing Fig. 5a–c, it is pretty clear that the results diverge concerning the stream that leads to the lowest IFT, although the figures show that injection of CO₂ with 50% methane causes the highest IFT. Figure 5b shows a clear trend that the higher the methane concentration in the injection stream, the higher the gas–oil IFT, in agreement with the results observed by Zhang et al. (2018) and Gu et al. (2013). However, Fig. 5a and c show that the lowest IFT is achieved by injecting CO₂ with 25% methane, indicating that there may be an optimal concentration that provides the maximum recovery. The disagreements found between the results obtained in this work and those from the literature are because, in the literature, the experiments for data collection consider only the oil and gas phases. In contrast, a water phase is also present in the system in the simulations performed in this work. The current work does not show the effects of the water phase on the gas–oil IFT. However, the IFT is a property directly affected by the phase's saturation. Therefore, the water phase affects the phase equilibrium and, consequently, the value of the IFT.

Furthermore, in the literature, experiments for data collection are carried out in a controlled environment so that the system pressure is independent of the methane content in the injection gas. However, as shown in Fig. 4, methane concentration in the injection gas directly affects the system pressure in a petroleum reservoir. Based on the apparent contradiction described above, the IFT depends on two significant variables: the block pressure, which increases as the methane content in the injection gas increases, and the CO₂ dissolution in oil, which decreases with the increase in methane concentration, as shown in Fig. 2. So, there is an offset effect acting on the system because the block pressure and the CO₂ dissolution in oil both cause a decrease in the IFT and are oppositely affected by the increase in the methane concentration. This offset explains why Fig. 5a and c have an optimal methane concentration, unlike Fig. 5b. Furthermore, it is also noted that Fig. 5b presents IFT values much higher than the others, which was expected since lower injection pressures usually lead to higher IFT values. As the IFT value is directly related to the difference between the phase densities, this result is consistent with what was observed in Fig. S4 in Section C in Supplementary Information. Figure 5c shows that, after reaching a stable region, the curve for pure CO₂ presents a drop toward the null value in 2013. This anomalous behavior is in line with expectations since, following the miscibility hypothesis, when the phases of a system become miscible, the interfaces cease to exist, and, consequently, the interfacial tension takes on a null

value (Abedini et al. 2014; Gu et al. 2013). Thus, when the IFT value drops, the system reaches the flow MMP, in this case, around 2014. In the same year, the black curve in Fig. S2.c in Section B, in Supplementary Information, reached its peak pressure, indicating that this abrupt increase in pressure led the system to the MMP, whose value is between the peak pressure and the pressure recorded in the previous year.

Analysis of the oil recovery

Once the behavior of several properties, including the IFT, were analyzed, it was finally possible to evaluate the oil recovery throughout the injection process and the effect of these properties on the recovery factor. Figure 6 presents the field oil recovery over time for the three sets of simulations and each of the different compositions of the injection gas. All the field oil recovery curves over time show an upward behavior, which was expected since, as time goes on, the amount of oil produced from the reservoir increases due to the gas injection process. However, in the first ten to twenty years of the injection process, it is possible to notice that the most significant recovery is achieved by using CO₂ with 50% methane. According to Fig. 6a and b, more remarkable recovery is favored by higher injection pressure due to the increased CO₂ dissolution in oil and, consequently, the decrease in the IFT, promoted by the increase in pressure, which also leads to the rise in the capillary number (Alotaibi and Nasr-El-Din 2009). The highest oil recoveries observed in this work are achieved considering a constant injection flow rate, as seen in Fig. 6c, when the injection gas is either 100% CO₂ or CO₂ with 25% methane. Comparing Figs. 5 and 6, it can be seen that, regardless of the methane content, the recovery curves tend to agree with the IFT curves, so the lower the IFT, the greater the recovery.

Figure 6c shows that the values achieved by oil recovery considering pure CO₂ (black curve) and CO₂ with 25% methane (blue curve) are the highest and close to each other, even with a difference in the values of IFT. This occurs because the system with 100% CO₂ injection achieved miscibility in 2013, which causes the black curve to drop to zero, although the IFT of the black curve generally presents higher values than the blue curve. This IFT drop brings the two oil recovery curves to such close values.

Regarding the effect of methane concentration on oil recovery, the greatest recovery tends to be achieved with 100% CO₂ injection since methane decreases the CO₂ solubility in oil. It agrees with the result of Fig. 6b and partially with that of Fig. 6c. However, Ghaffar (2016) observed that, under a condition of less injected pore volume, the injection of CO₂ with 15% methane provides the greatest recovery, which partly agrees with the results of Fig. 6a and c. Comparing the results obtained in the present work, which considers recovery as

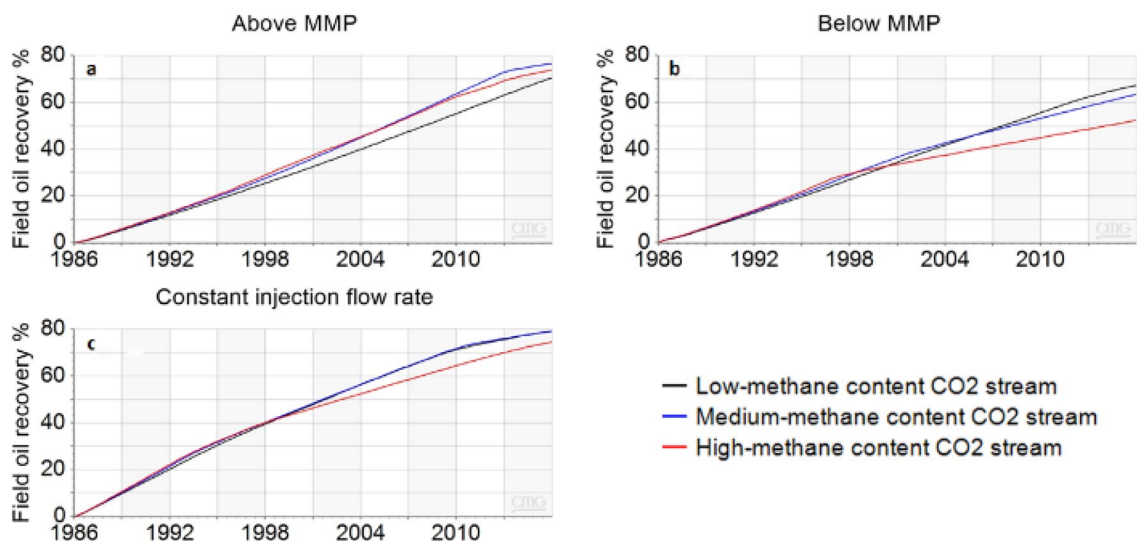


Fig. 6 Field oil recovery over time, considering the three sets of simulations and the three different methane concentrations in the CO₂ injection stream

a function of time, with the results of Ghaffar (2016), who believes it is a function of the injected pore volume, both are expressions of the same variable. Considering this and comparing the results of Ghaffar (2016) with those in Fig. 6b and c, it is noted that, at the beginning of the injection process (the first ten years), the greatest recovery is achieved by injecting CO₂ + methane. However, as the injection progresses, the most significant recovery tends to be performed by injecting 100% CO₂, although Fig. 6a shows a greater recovery for a CO₂ + methane injection. In Fig. 6a, the slope of the curves for CO₂ + methane injection decreases, while for pure CO₂, it remains constant. Such behavior indicates that given enough time, oil recovery considering pure CO₂ exceeds recovery for CO₂ + methane, thus agreeing with what was observed for the other figures. Ghaffar (2016) does not explain this difference in recovery behavior. Nevertheless, based on the results observed in the present study, it can be concluded that the offset effect of methane concentration on the pressure and CO₂ solubility is mainly responsible for this performance. This result also means that by increasing the injection time, the curve considering a 100% CO₂ injection yields the highest recovery. Thus, pure CO₂ injection seems more advantageous in the long term. Still, an optimal methane concentration in the CO₂ injection stream maximizes the recovery in the first years of injection.

Conclusions

The present work performed an extensive analysis of the effect of the methane content in the CO₂ injection stream on relevant variables of EOR processes, stressing the role of the interfacial tension and its relationship with the fluid flow

through the reservoir. The behavior of IFT and other related properties of the gas–oil system was evaluated over time instead of considering only static systems typically found in the literature. Some of the unprecedented results include the opposite effects of methane concentration on the CO₂ stream and the change in the impact of methane concentration on oil recovery over time. The simulations carried out under these conditions show that the effect of the methane content on the gas–oil IFT in a CO₂ injection process is somewhat tricky. An offset was observed between the effects of increased methane content in the injection gas on many properties. For instance, an increase in the methane content leads to a higher internal reservoir pressure that causes a reduction in the IFT, and to a lower CO₂ dissolution in oil that raises the IFT. The balance between these opposite effects can explain why the IFT presents a lower value either for 100% CO₂ injection or a mixture of CO₂ + methane injection. The simulations also indicate that higher oil recovery is favored by higher injection pressure in the case of CO₂ injection at constant pressure, but the highest recovery factor was obtained for CO₂ injection at a constant flow rate. The methane content effect on oil recovery varies over time. “In the long term, the highest recovery seems to be achieved by injecting CO₂ with as least methane as possible.”

Nonetheless, an optimal methane concentration provides maximum recovery at the beginning of the injection process. The variation of oil recovery over time is also caused by the balance between these opposite effects due to increased injection gas methane content. Although a simple relationship between the methane concentration in the injection gas and the oil recovery factor was not obtained, it is possible to say that the lower the IFT, the greater the recovery. This

result confirms that the interfacial tension is one of the key properties of the enhanced oil recovery process by CO₂ injection because there is a remarkable agreement between the capillary number and IFT values. Consequently, it is possible to monitor the CO₂ injection process along with the fluid flow through the reservoir by observing the behavior of properties such as IFT, phase densities, and internal pressure over time.

Supplementary Information The online version contains supplementary material available at <https://doi.org/10.1007/s43153-023-00329-8>.

Acknowledgements The authors acknowledge the support by the Agência Nacional de Petróleo, Gás Natural e Biocombustíveis (ANP), and the Petrogal Brasil S.A., related to the grant from the research and development rule, as well as the Engineer Juan Alberto Mateo Hernandez (CMG).

Data availability No data was used for the research described in the article.

Declarations

Conflict of interest On behalf of all authors, the corresponding author states that there is no conflict of interest.

References

- Abdullah N, Hasan N (2021) Effects of miscible CO₂ injection on production recovery. *J Pet Explor Prod Technol* 11(9):3543–3557. <https://doi.org/10.1007/s13202-021-01223-0>
- Abedini A, Mosavat N, Torabi F (2014) Determination of minimum miscibility pressure of crude Oil-CO₂ system by oil swelling/extraction test. *Energy Technol* 2(5):431–439. <https://doi.org/10.1002/ente.201400005>
- Alotaibi MB, Nasr-El-Din HA (2009) Effect of brine salinity on reservoir fluids interfacial tension. Society of Petroleum Engineers - EUROPEC/EAGE Conference and Exhibition 2009, June, 8–11. <https://doi.org/10.2118/121569-MS>
- Cahn JW, Hilliard JE (1958) Free energy of a nonuniform system. I. Interfacial free energy. *J Chem Phys* 28(2):258–267. <https://doi.org/10.1063/1.1744102>
- Carvalho AS, Costa GMN, de Melo SABV (2019) Simulation of enhanced oil recovery in pre-salt reservoirs: The effect of high CO₂ content on low salinity water alternating gas injection. Society of Petroleum Engineers - Reservoir Characterisation and Simulation Conference and Exhibition 2019, September, 17–19. <https://doi.org/10.2118/196684-ms>
- Cheng P, Li D, Boruvka L, Rotenberg Y, Neumann AW (1990) Automation of axisymmetric drop shape analysis for measurements of interfacial tensions and contact angles. *Colloids Surf* 43(2):151–167. [https://doi.org/10.1016/0166-6622\(90\)80286-D](https://doi.org/10.1016/0166-6622(90)80286-D)
- Cho J, Park G, Kwon S, Lee KS, Lee HS, Min B (2020) Compositional modeling to analyze the effect of CH₄ on coupled carbon storage and enhanced oil recovery process. *Appl Sci* 10:4272. <https://doi.org/10.3390/app10124272>
- Choubineh A, Helalizadeh A, Wood DA (2019) The impacts of gas impurities on the minimum miscibility pressure of injected CO₂-rich gas-crude oil systems and enhanced oil recovery potential. *Pet Sci* 16(1):117–126. <https://doi.org/10.1007/s12182-018-0256-8>
- Christensen JR, Stenby EH, Skauge A (2001) Review of WAG field experience. *SPE Reserv Eval Eng* 4(02):97–106. <https://doi.org/10.2118/71203-PA>
- Drexler S, Correia EL, Jerdy AC, Cavadas LA, Couto P (2020) Effect of CO₂ on the dynamic and equilibrium interfacial tension between crude oil and formation brine for a deepwater pre-salt field. *J Petrol Sci Eng.* <https://doi.org/10.1016/j.petrol.2020.107095>
- Firoozabadi A, Katz DL, Soroosh H, Sajjadian VA (1988) Surface tension of reservoir crude-oil/gas systems recognizing the asphalt in the heavy fraction. *SPE Reserv Eng* 3(01):265–272. <https://doi.org/10.2118/13826-PA>
- Gajbhiye R (2020) Effect of CO₂/N₂ mixture composition on interfacial tension of crude oil. *ACS Omega* 5(43):27944–27952. <https://doi.org/10.1021/acsomega.0c03326>
- Ghaffar A (2016) Role of impurities in CO₂ stream during CO₂ injection process in heavy oil systems. 145. <http://ourspace.uregina.ca/handle/10294/6824>
- Green DW, Willhite GP (2018) Enhanced oil recovery system. Richardson, Texas
- Gu Y, Hou P, Luo W (2013) Effects of four important factors on the measured minimum miscibility pressure and first-contact miscibility pressure. *J Chem Eng Data* 58(5):1361–1370. <https://doi.org/10.1021/je4001137>
- Hashemi Fath A, Pouranfard AR (2014) Evaluation of miscible and immiscible CO₂ injection in one of the Iranian oil fields. *Egypt J Pet* 23(3):255–270. <https://doi.org/10.1016/j.ejpe.2014.08.002>
- Hemmati-Sarapardeh A, Ayatollahi S, Ghazanfari MH, Masihi M (2014) Experimental determination of interfacial tension and miscibility of the CO₂-crude oil system; temperature, pressure, and composition effects. *J Chem Eng Data* 59(1):61–69. <https://doi.org/10.1021/je400811h>
- Islam MR (2019) Greening of enhanced oil recovery. Economically and environmentally sustainable enhanced oil recovery. Scrivener, Beverly, pp 525–662. <https://doi.org/10.1002/9781119479239.ch7>
- Jin L, Pekot LJ, Hawthorne SB, Gobran B, Greeves A, Bosshart NW, Jiang T, Hamling JA, Gorecki CD (2017) Impact of CO₂ impurity on MMP and Oil Recovery performance of the Bell Creek Oil Field. *Energy Procedia* 114:6997–7008. <https://doi.org/10.1016/j.egypro.2017.03.1841>
- Killough JE, Kossack CA (1987) Fifth comparative solution project: evaluation of miscible flood simulators. In SPE Symposium on Reservoir Simulation (p. SPE-16000-MS). <https://doi.org/10.2118/16000-MS>
- Ligero EL (2011a) ATCE 2011: Emprego de CO₂ em Métodos de EOR e seu Efeito em Carbonatos UNISIM ON-LINE. https://www.unisim.cepetro.unicamp.br/online/UNISIM_ON_LINE_N62.PDF
- Ligero EL (2011b) Modelagem Trifásica da Histerese na Simulação Composicional da Injeção WAG-CO₂. UNISIM ON-LINE, 1(7). https://www.unisim.cepetro.unicamp.br/online/UNISIM_ON_LINE_N83.PDF
- Nobakht M, Moghadam S, Gu Y (2007) Effects of viscous and capillary forces on CO₂ enhanced oil recovery under reservoir conditions. *Energy Fuels* 21(6):3469–3476. <https://doi.org/10.1021/ef700388a>
- Pereira LMC (2016) Interfacial tension of reservoir fluids: an integrated experimental and modelling investigation. July, p 215. <http://hdl.handle.net/10399/3207>
- Perera MSA, Gamage RP, Rathnaweera TD, Ranathunga AS, Koay A, Choi X (2016) A Review of CO₂-Enhanced oil recovery with a simulated sensitivity analysis. *Energies* 9(7):481. <https://doi.org/10.3390/en9070481>
- Sequeira DS, Ayirala SC, Rao DN (2008) Reservoir condition measurements of compositional effects on gas-oil interfacial tension and miscibility. Society of Petroleum Engineers - Symposium on

- Improved Oil Recovery 2008, April, 20–23. <https://doi.org/10.2118/113333-MS>
- Shang Q, Xia S, Shen M, Ma P (2014) Experiment and correlations for CO₂–oil minimum miscibility pressure in pure and impure CO₂ streams. *RSC Adv* 4(109):63824–63830. <https://doi.org/10.1039/c4ra11471j>
- Shokrollahi A, Arabloo M, Gharagheizi F, Mohammadi AH (2013) Intelligent model for prediction of CO₂–Reservoir oil minimum miscibility pressure. *Fuel* 112:375–384. <https://doi.org/10.1016/j.fuel.2013.04.036>
- Weinaug CF, Katz DL (1943) Surface tensions of methane-propane mixtures. *Ind Eng Chem* 35(2):239–246. <https://doi.org/10.1021/ie50398a028>
- Zanganeh P, Ayatollahi S, Alamdari A, Zolghadr A, Dashti H, Kord S (2012) Asphaltene deposition during CO₂ injection and pressure depletion: a visual study. *Energy Fuels* 26(2):1412–1419. <https://doi.org/10.1021/ef2012744>
- Zhang PY, Huang S, Sayegh S, Zhou XL (2004) Effect of CO₂ Impurities on gas-injection EOR processes. *SPE/DOE Symposium on Improved Oil Recovery 2004*, April, 17–21. <https://doi.org/10.2118/89477-MS>
- Zhang K, Tian L, Liu L (2018) A new analysis of pressure dependence of the equilibrium interfacial tensions of different light crude oil–CO₂ systems. *Int J Heat Mass Transf* 121:503–513. <https://doi.org/10.1016/j.ijheatmasstransfer.2018.01.014>
- Zhao Y, Yu Q (2018) Effect of CH₄ on the CO₂ breakthrough pressure and permeability of partially saturated low-permeability sandstone in the Ordos Basin, China. *J Hydrol.* <https://doi.org/10.1016/j.jhydrol.2017.11.030>
- Zick AA (1986) Combined condensing/vaporizing mechanism in the displacement of oil by enriched gases. *Society of Petroleum Engineers - Annual Technical Conference and Exhibition October, 1986*, 5–8. <https://doi.org/10.2523/15493-ms>
- Zuo YX, Stenby EH (1996) A linear gradient theory model for calculating interfacial tensions of mixtures. *J Colloid Interface Sci* 182(1):126–132. <https://doi.org/10.1006/JCIS.1996.0443>
- Zuo YX, Stenby EH (1997) Corresponding-States and Parachor Models for the calculation of interfacial tensions. *Can J Chem Eng* 75(6):1130–1137. <https://doi.org/10.1002/cjce.5450750617>

Publisher's Note Springer Nature remains neutral with regard to jurisdictional claims in published maps and institutional affiliations.

Springer Nature or its licensor (e.g. a society or other partner) holds exclusive rights to this article under a publishing agreement with the author(s) or other rightsholder(s); author self-archiving of the accepted manuscript version of this article is solely governed by the terms of such publishing agreement and applicable law.